

Metal-coated Si springs: Nanoelectromechanical actuators

J. P. Singh,^{a)} D.-L. Liu, D.-X. Ye, R. C. Picu,^{b)} T.-M. Lu, and G.-C. Wang

Department of Physics, Applied Physics and Astronomy, Rensselaer Polytechnic Institute, Troy, New York 12180-3590

(Received 11 November 2003; accepted 15 March 2004; published online 20 April 2004)

We demonstrated a nanoscale electromechanical actuator operation using an isolated nanoscale spring. The four-turn Si nanosprings were grown using the oblique angle deposition technique with substrate rotation, and were rendered conductive by coating with a 10-nm-thick Co layer using chemical vapor deposition. The electromechanical actuation of a nanospring was performed by passing through a dc current using a conductive atomic force microscope (AFM) tip. The electromagnetic force leads to spring compression, which is measured with the same AFM tip. The spring constant was determined from these measurements and was consistent with that obtained from a finite element analysis. © 2004 American Institute of Physics. [DOI: 10.1063/1.1738935]

Nanostructures such as nanorods, nanowires, and nanosprings are building blocks of future nanomachines and have potential applications in nanosensors and nanodevices.¹ Among them, the helical nanosprings have recently attracted much attention in the nanoscience community.^{2–8} The elastic properties of individual nanosprings⁸ and of an ensemble of nanosprings⁹ have been reported. Due to their high structural flexibility and strength, nanosprings should be suitable for applications in nanoelectromagnetic sensors and devices. However, so far no electromechanically actuated nanosprings have been demonstrated.

In this letter we present the results of electromechanical actuation of individual helical Si nanosprings. The four-turn amorphous Si nanosprings were rendered conductive by coating with a thin layer of Co using the chemical vapor deposition (CVD) technique. A dc current is passed through the nanospring by a conductive atomic force microscope (AFM) tip. The electromagnetic force in the coil puts the nanospring in compression. The total deformation of the nanospring is measured with the same AFM tip held in contact mode at the top of the nanospring.

The Si nanosprings were grown on a templated substrate by the oblique angle deposition technique with substrate rotation.^{10,11} The template consists of a two-dimensional array of W posts arranged in a square pattern (by a deep UV lithographic technique). The cylindrical W posts have an average top diameter of 150 nm, while the bottom diameter is about 360 nm. The height of an individual post is about 450 nm and the post-to-post distance is about 1000 nm. Four-turn nanosprings were grown on these W posts. The deposition was performed in a high vacuum chamber with a base pressure of 5×10^{-5} Pa. The Si source (99.999%, Alfa Aesar, USA) was evaporated from a graphite crucible by electron bombardment heating. The vapor flux arrived at a fixed oblique incidence angle of 85° from the substrate normal. The deposition rate was 0.55 nm/s. The substrate was mounted 32 cm above the source. The average substrate rotational speed was 2 h/turn and each turn was divided into four discrete steps. The rotational angle was fixed for half an hour growth and then rotated by 90° for the next half an hour growth.

Nanosprings with a rise angle of 13.6° and a pitch h of 1095 ± 38 nm resulted. The nanospring wire diameter t and outer coil diameter $2R$ were determined to be 343 ± 33 and 1091 ± 56 nm, respectively. The helical Si nanosprings were coated with about 10 nm thick Co by CVD. The thickness of the Co layer was determined by Rutherford backscattering of Co coated blanket Si substrate placed next to the Si nanospring sample. The source was dicobalt octacarbonyl, $\text{Co}_2(\text{CO})_8$ and the deposition was performed in a vertical reactor. The sample was heated up to 80°C during deposition. The base pressure of the reactor was about 2×10^{-1} Pa. The total reaction time was 5 min.

A Park Scientific AFM was used for the electromechanical actuation of the nanosprings in ambient conditions. The AFM Si cantilever with a monocrystalline Si conical tip used in these measurements has a spring constant of 17 N/m. In order to be rendered conductive, the tip was coated with 30 nm Pt by sputtering while insuring that the opposite surface of the cantilever, where the laser beam of the AFM reflects, remains uncoated. The tip size and vertical scale were calibrated before the measurements using a standard tip characterization Si grating. The radius of curvature of the tip was found to be about 60 nm.

Figure 1 shows a cross sectional scanning electron microscopy image of the Co coated helical Si nanosprings and a schematic showing the circuit used for the electromechanical measurements using a conducting AFM tip. Also shown is a schematic detailing the structure of the Co coated Si

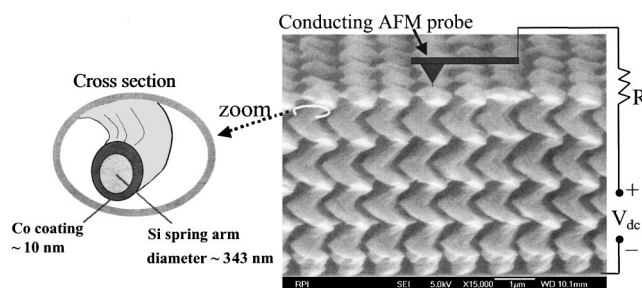


FIG. 1. Cross sectional SEM image of four-turn Si nanosprings. A schematic of the circuit used for the electromechanical measurements including a Pt (30 nm) coated AFM tip, a resistor R (200–500 Ω) and a dc power supply V_{dc} (0–24 V) is also shown. The schematic on the left shows the cross section of the conductive Co coating on the Si nanospring.

^{a)}Electronic mail: singhj@rpi.edu

^{b)}Department of Mechanical, Aerospace and Nuclear Engineering.

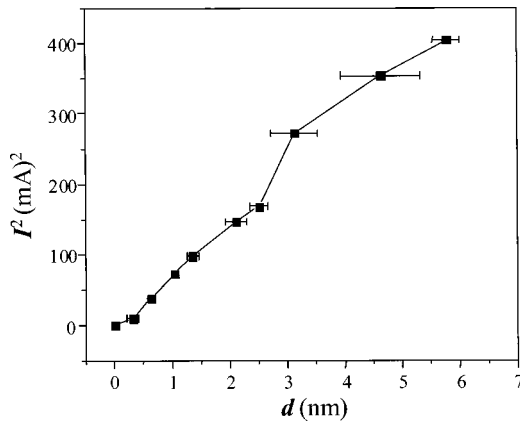


FIG. 2. I^2 vs nanospring compressive displacement d curve showing the electromechanical behavior of a single nanospring. The magnetic force is proportional to I^2 . Each data point is the average of ten measurements on a nanospring. Each error bar on the measured nanospring compression d on the curve represents the standard deviation of the measured value.

nanospring. First, the topography of nanosprings sample was imaged by using the noncontact AFM mode. This allowed us to precisely select a position on an isolated single nanospring. Then, the AFM mode was changed from noncontact to contact mode and a preset constant force of 1 nN was applied. The preset force is small enough to avoid overloading the structure. A dc current I passed from the conducting AFM tip to the isolated nanospring. The current generates a magnetic field \mathbf{B} that produces a magnetic force \mathbf{F} between the coils of the nanospring and compresses the spring. Since the AFM was operated in the constant force mode, the z scanner on which the spring is mounted moved a distance d to compensate the spring compression. We recorded the spring compression d as a function of the applied current. The experimental plot of I^2 versus the total measured compressive displacement of the nanospring d is shown in Fig. 2. Each data point is the average of ten different measurements on the particular nanospring. The error bars on d represent the standard deviation of the measured value. As expected, the magnetic force experienced by the nanospring is propor-

tional to I^2 . At steady state equilibrium, this magnetic force is balanced by the spring elastic force \mathbf{F}_s .

To test the effect of an applied current-generated heating on the nanostructure, we used vertical Si nanorods grown by the same oblique angle deposition technique and the nanorods were then coated with a 10 nm thick Co film by chemical vapor deposition. The thermal expansion of a vertical nanorod is expected to be more obvious than that of a spring since the electromechanical effect is eliminated. We have not observed any noticeable thermal expansion or contraction under applied currents similar to those used in the nanospring measurements. We have seen a slight increase of the noise in the cantilever deflection signal ranging from ± 0.2 to ± 0.5 nm after applying 20 mA current to the nanorod. This value is much smaller than d measured in the electromechanical test under a similar current.

In order to evaluate the electromagnetic forces acting on the structure, the actual spring was modeled as a coil of pitch h and diameter $2R$ equal to those of the physical structure, and of vanishing wire diameter. This is equivalent with assuming that the whole current flows through an infinitesimally thin wire that follows the geometry of the real spring. The electromagnetic interactions generate distributed forces on the wire. The force between two infinitesimal segments of vectors $d\mathbf{l}_1$ and $d\mathbf{l}_2$ may be evaluated with the equation¹²

$$d\mathbf{F} = \Lambda \frac{d\mathbf{l}_2 \times [d\mathbf{l}_1 \times (\mathbf{r}_2 - \mathbf{r}_1)]}{|\mathbf{r}_2 - \mathbf{r}_1|^3}, \tag{1}$$

where $\Lambda = \mu_0 \mu_r I^2 / (4\pi)$ and \mathbf{r}_1 and \mathbf{r}_2 are the position vectors of the two segments. μ_0 is the permeability of free space, and μ_r is the relative permeability of Co for which we assume a value of 200 (the values reported in the literature range from 70 to 250).¹³

Let us consider a cylindrical coordinate system with the z axis aligned with the axis of the coil and the $\theta=0$ position corresponding to the lower end of the spring. The force on an element of the spring of length $R\sqrt{1+\xi^2}d\theta$ can be expressed in this coordinate system as

$$\frac{(dF_r, dF_\theta, dF_z)}{\Lambda} = d\theta \int_{-\theta}^{8\pi-\theta} \frac{(\xi^2 + (1-\xi^2)\cos\eta - \cos^2\eta, \xi^2\eta + (1-\xi^2)\sin\eta - \sin\eta\cos\eta, \xi\sin\eta - \xi\eta\cos\eta)}{(2-2\cos\eta + \xi^2\eta^2)^{3/2}} d\eta, \tag{2}$$

where, the dimensionless parameters ξ and η are given by $\xi = h/(2\pi R)$ and $\eta = \theta' - \theta$. The evaluation of this integral provides the distributed force on the wire in the radial, tangential, and axial directions, as a function of θ and the geometrical parameter ξ . The angle θ ranges from 0, corresponding to the lower end of the spring, to 8π , corresponding to the upper end (for a four-turn spring). The geometrical parameter ξ ranges from 0.29 to 0.34 as evaluated based on the measured extreme spring dimensions.

The right-hand side of Eq. (2) is dimensionless as Λ has units of force. The distribution was evaluated numerically by performing the integration. As expected, an infinite spring

would carry no axial or tangential forces, due to the symmetry. In the present case however, the spring is loaded due to the unbalance of forces at the upper and lower ends. The force distribution at the two ends is similar, but the force signs are opposite to each other (action–reaction). The radial and tangential components of the unbalance force acting at the ends put the spring in bending. The axial component of the unbalance force loads the structure in the axial direction. It is interesting to note that for large ξ values ($\xi > 0.5$) corresponding to open coils with large pitch values, the axial force results to be tensile, while for small ξ , it is compressive. At the same time, the bending becomes significant when ξ is

large, while for $\xi < 0.2$, its effect is negligible compared with that of the axial load.

For $\xi = 0.3$, the actual distribution of electromagnetic forces produces an end effect which may be represented by three concentrated forces acting at the upper end of the spring, two in the plane perpendicular to the axial direction, F_x and F_y , and an axial, compressive force, F_z . Here, the Cartesian x axis is aligned with the $\theta = 0$ direction. The forces are $F_x = -0.95\Lambda$, $F_y = 0.63\Lambda$, and $F_z = -1.47\Lambda$. The compression of the spring in the z direction due to the axial force is given by F_z/κ , where κ is the spring constant. In order to evaluate the displacement of the upper end of the spring due to bending (induced by F_x and F_y), the spring was modeled with finite elements. The material of the spring was taken to be linear elastic with Young's modulus and Poisson's ratio of 45 GPa and 0.22, respectively.^{8,14} The total deflection of the upper end of the spring results as the sum of the deflections induced by the axial force and that due to bending and evaluated using the finite element model for F_x and F_y . This quantity is to be compared with the measured compressive displacement d corresponding to various currents I (and therefore to various Λ) in Fig. 2. By imposing this equivalence, the spring constant is evaluated to be 3 N/m.

It should be observed that a certain uncertainty exists with regard to the exact path over which the current flows. The approximation made in the evaluation of the electromagnetic force according to which the whole current flows through an infinitesimally thin wire, may induce errors. We propose that an upper limit of the electromagnetic force may be evaluated by assuming that the relevant pitch, corresponding to the distance between two neighboring conductive paths, is $h - t$, i.e., the distance from the upper surface of the wire at $\theta = 0$ to the lower surface of the wire at $\theta = 2\pi$. With this assumption, $\xi = 0.18$. For this value of the geometrical parameter, the bending may be neglected with respect to the effect of the axial force. The total compression of the structure results as $d = -8.1\Lambda/\kappa$. Requiring the compatibility with the data in Fig. 2, the spring constant results to be $\kappa = 12$ N/m.

In order to obtain an independent evaluation of the spring constant, mechanical measurements similar to those reported in our previous work were performed.⁸ In these measurements, no electrical current is passed through the structure, rather the springs are loaded in compression using the AFM tip. Representative loading (filled triangles) and unloading (open squares) curves obtained for a single nanospring are shown in Fig. 3. The response of the structure is linear and the loading and unloading curves overlap. No indentation was observed on the surface of the nanospring after testing. The spring constant is determined from the slope of (best fit to) the characteristic curve in Fig. 3 to be $\sim 8.75 \pm 0.04$ N/m. Note that the mechanical force from the AFM tip applied on the wire of the spring is loaded off-axis. We have also performed finite element analysis to clarify this point. Considering the uncertainty in the dimensional parameters, the apparent stiffness for loading with a force applied on the wire ranges from 5.2 to 17 N/m. Therefore our force constant measured by AFM is consistent with the modeling.

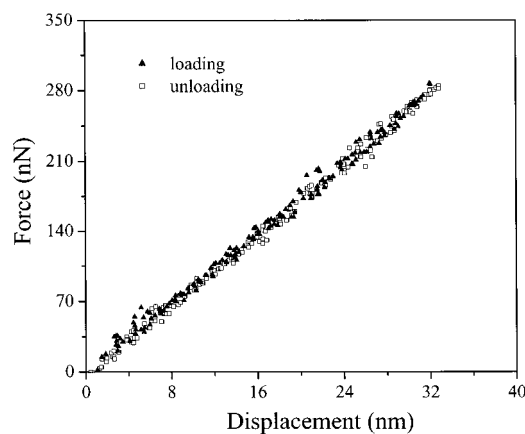


FIG. 3. Force vs nanospring displacement curves for a single nanospring. Filled triangles represent the loading and open squares represent the unloading of the AFM tip during mechanical measurement. The slope gives the spring constant.

When the force is applied axially, the computed spring constant ranges from 10 to 32 N/m. The difference is due to the fact that off-axis loading produces both spring compression and bending, while axial loading produces compression only. This finite element result is consistent with our previous work.⁸ The experimental values of the spring constant obtained from the mechanical testing method are of the same order of magnitude with those resulting from the electromechanical tests.

In conclusion, we have shown that it is possible to electromechanically actuate a nanoscale structure such as a nanospring. Within the accuracy of our measurements and modeling, its behavior appears to be similar to that of equivalent macroscopic devices.

The work was supported by the NSF through Grant No. CMS0324492. The authors thank Paul Morrow and Tansel Karabacak for valuable discussions and P.-K. Lim for providing us the template.

¹M. Roukes, *Phys. World* **14**, 25 (2001).

²Y.-P. Zhao, D.-X. Ye, Pei-I Wang, G.-C. Wang, and T.-M. Lu, *Int. J. Nanosci.* **1**, 87 (2002).

³D. N. McIlroy, D. Zhang, Y. Kranov, and M. G. Norton, *Appl. Phys. Lett.* **79**, 1540 (2001).

⁴X. Chen, S. Zhang, D. A. Dikin, W. Ding, R. S. Ruoff, L. Pan, and Y. Nakayama, *Nano Lett.* **3**, 1299 (2003).

⁵S. R. Kennedy, M. J. Brett, O. Toader, and S. John, *Nano Lett.* **2**, 59 (2002).

⁶S. Motojima, M. Kawaguchi, K. Nozaki, and H. Iwanaga, *Appl. Phys. Lett.* **56**, 321 (1990).

⁷T. Hayashida, L. Pan, and Y. Nakayama, *Physica B* **323**, 352 (2002).

⁸D.-L. Liu, D.-X. Ye, F. Khan, F. Tang, B.-K. Lim, R. C. Picu, G.-C. Wang, and T.-M. Lu, *J. Nanosci. Nanotechnol.* **3**, 492 (2003).

⁹M. W. Seto, K. Robbie, D. Vick, M. J. Brett, and L. Kuhn, *J. Vac. Sci. Technol. B* **17**, 2172 (1999).

¹⁰K. Robbie, M. J. Brett, and A. Lakhtakia, *Nature (London)* **384**, 616 (1996); and references therein.

¹¹Y.-P. Zhao, D.-X. Ye, G.-C. Wang, and T.-M. Lu, *Nano Lett.* **2**, 351 (2002).

¹²D. J. Griffiths, *Introduction to Electrodynamics* (Prentice-Hall, Englewood Cliffs, NJ, 1981), p. 215.

¹³E. U. Condon and H. Odishaw, *Handbook of Physics* (McGraw-Hill, New York, 1958), Chap. 8.

¹⁴T. Searle, *Properties of Amorphous Si and its alloys* (Inspec, London, 1998), p. 359.